Optimum Integration of Solar Energy With Battery Energy Storage Systems

Yaze Li, *Student Member, IEEE*, and Jingxian Wu, *Senior Member, IEEE*

***Abstract*—This article discusses optimum designs of photovoltaic (PV) systems with battery energy storage system (BESS) by using real-world data. Specifically, we identify the optimum size of PV panels, the optimum capacity of BESS, and the optimum scheduling of BESS charging/discharging, such that the long-term overall cost, including both utility bills and the PV system, is minimized. The optimization is performed by considering a plethora of parameters, such as energy usage, energy cost, weather, geographic location, inflation, and the cost, efficiency, and aging effects of solar panels and BESS. To capture the impacts of long-term factors such as aging effects, inflation, and discounted economic returns, the problem is formulated as a mixed integer nonlinear programming (MINLP) problem over the time horizon covering the entire life cycles of solar panels and BESS of the order of ten years or longer, whereas almost all existing works on PV system designs consider much shorter time horizons of the order of days or weeks. The MINLP is transformed into mixed integer linear programming (MILP) and solved by branch-and-bound (B&B) algorithm. The complexity of MILP is high due to the long time horizon. A new low-complexity algorithm is then proposed by using dynamic programming, where it is shown that the MINLP problem can be transformed into one that satisfies Bellman's principal of optimality. Applying the newly developed algorithms on real-world data from a commercial user in San Francisco reveals that the system achieves the break-even point at the 66th month and achieves a 29.3% reduction in total system cost.**

***Index Terms*—Battery energy storage system (BESS), demand charge, dynamic programming (DP), mixed integer nonlinear programming (MINLP), photovoltaic (PV), time of use (TOU).**

I. Introduction

SOLAR power is a clean, inexpensive, and renewable energy source that is widely adopted around the world. One of the most efficient ways to harness solar power is through photovoltaic (PV) cells, or solar panels, which convert light directly into electricity using photoelectric effects. The state of California in the United States of America mandates solar panels on the roofs of all new homes starting in 2020 [1]. The growing popularity and constantly increasing demands of solar energy necessitate optimum designs of PV systems that can be seamlessly integrated in power grids and achieve maximum savings in energy and overall system cost.

The variability, uncertainty, and nonsynchronous generation of PV power sources impose numerous challenges on the large-scale and cost-effective deployment of PV systems [2]. The intermittent and stochastic nature of solar energy creates an imbalance between energy supplies and demands. Such an imbalance can be partly compensated by integrating the PV system with battery energy storage system (BESS). The BESS can store excessive solar energy during off-peak hours and discharge the stored energy during high-demand hours, such that both energy usage and peak demands can be significantly reduced.

There have been growing interests in the optimum designs and scheduling of energy systems with energy storage devices (ESS). Most designs aim at minimizing the energy cost or operating cost through optimum scheduling of energy generation and/or storage. In [3], the optimum scheduling of a pump-storage hydropower station is formulated as a mixed integer linear programming (MILP) problem, where the nonlinearity of power generation in hydroturbines is approximated by a piecewise linear function. In [4], the optimum scheduling of distributed energy resources (DER) is formulated as a linear programming (LP) problem to reduce operation cost and to shave peak demands. In [5], the optimum scheduling of behind-the-meter ESS is formulated as a mixed integer nonlinear programming (MINLP) problem, and the problem is equivalently transformed into an LP by introducing auxiliary variables. The complexity of LP-based approaches scales, in general, in polynomial time with respect to the number of decision variables and constraints. The complexity could be prohibitively high when the number of decision variables is large.

Optimum ESS scheduling can also be solved by using dynamic programming (DP), which relies on Bellman's principle of optimality to decompose the original problem into a sequence of simpler subproblems in a recursive manner [6]–[11]. In the optimum designs of ESS systems, the state variables are usually states of charge of the ESS, which often need to be discretized for an efficient solution [6]. For utility bill minimization, the demand charge introduces a supremum term in the objective function, which violates Bellman's principal of optimality necessary for DP. This problem is solved by using the concept of forward separable function with augmented state variables in [11], or multiobjective DP in [9]. The integration of ESS system with renewable energy sources adds new degrees-of-freedom that can further improve the efficiency of energy usage. The optimum design of power systems with both ESS and renewable

Manuscript received May 8, 2019; revised October 2, 2019; accepted January 21, 2020. This work was supported in part by the U.S. National Science Foundation (NSF) under Grant ECCS-1711087 and in part by the Department of Energy under Award DE-OE0000779. Review of this manuscript was arranged by Department Editor T. Hong. *(Corresponding author: Yaze Li.)*

The authors are with the Department of Electrical Engineering, University of Arkansas, Fayetteville, AR 72701 USA (e-mail: yazeli@email.uark.edu; wuj@uark.edu).

Color versions of one or more of the figures in this article are available online at http://ieeexplore.ieee.org.

Digital Object Identifier 10.1109/TEM.2020.2971246

energy sources are discussed in [8] and [12], which consider the interactions of a variety of renewable energy sources and ESS devices, including PV panels, wind turbines, hydroelectric plants, pumping stations, etc.

The optimizations in most existing works are performed by assuming a fixed-sized ESS. In the design of battery-assisted PV systems, the optimum capacity of BESS and the number of solar panels are important decision parameters, and their optimum values are in general not readily available beforehand. The costs of solar panels and BESS accounts for a large amount of initial investment. The optimum designs need to ensure that the cost saving due to ESS and renewable energy sources can outweigh the system cost in the long run, thus the system cost should be a critical parameter in the system design. The operation cost and wear-out cost of the system are included in the formulations in [4], [5], and [8]. However, the initial procurement and installation costs are not considered in those works.

In addition to system cost, the optimum design should also consider aging effects of the devices, where the efficiencies and/or capacities of both solar panels and batteries degrade gradually over time [13]. To accurately model the aging effects, the optimization needs to be performed over a time horizon over the entire life cycles of batteries and solar panels. However, the time horizon in many existing works are one day [14], and multiday costs are obtained by multiplying the daily cost by the number of days [12], [15]. A 24-month dataset is used in [16], but with the assumption that the battery is fully charged at the beginning of each day. Thus, the optimization horizon is still within one day. In [3] and [5], the time horizon is extended to one month. A one-year optimization horizon is considered in [17] without considering the aging effects. In [18], the design is performed over a three-year optimization period, which is still shorter than the device life cycles, and it only considers the battery cycling aging effects.

In this article, we propose to perform optimum designs of battery-assisted PV systems by including system costs, aging effects of batteries and solar panels, inflation of electricity costs, and discounted long-term returns as design parameters. Unlike most previous works with short optimization horizons and nonaging models, the proposed research considers cycling aging and calendar aging of the batteries and solar panels. The optimum designs of the system are determined by a plethora of parameters, such as the load and weather data, utility rates, the cost of system procurement, installation, and maintenance, inflation rates, discounted long-term returns, and the charging/discharging schedules. The objective of the design is to minimize the long-term total cost of the system, including both system cost and utility cost in an engineering economic model, subject to physical limits of the batteries and solar panels, such as finite capacity, finite charging/discharging rates, efficiency depreciation over time, etc. In order to model and quantify the impacts of aging effects, the optimization time horizon covers a duration of ten years corresponding to the life cycles of batteries and solar panels. The problem is formulated as an MINLP with the number of optimization variables proportional to the optimization time horizon. Two solutions to the problems are proposed—one is based on MILP, and the other one is based on DP. The MILP-based solution can obtain the globally optimum solution with the help of the branch-and-bound (B&B) algorithm. However, the complexity of MILP-based solution grows in polynomial time with respect to the optimization horizon, and it becomes prohibitively high over long time horizons. The DP-based solution can achieve a balanced tradeoff between accuracy and complexity. Comparisons between the MILP- and DP-based solutions demonstrate that the DP-based solution can achieve similar performance as the MILP-based solution, but with a complexity that is only linear in optimization time horizon. The optimum designs are applied to real-world data from a large hotel in San Francisco [19], and it is shown that employing BESS in a PV system can achieve significant cost savings over PV-only system or conventional systems with no renewable energy sources.

The rest of this article is organized as follows. The system model and problem formulation are given in Section II. The MILP- and DP-based solutions are proposed in Sections III and IV, respectively. Section V presents the results obtained from case studies with real-world data. Finally, Section VI concludes this article.

II. System Model and Problem Formulation

In this section, we first present the model of the solar energy system. Based on the system model, the optimum design is formulated as an MINLP.

A. Battery Model

The time is divided into short nonoverlapping windows with duration τ each, e.g., $\tau = 1$ h. The state of charge (SOC), or the energy stored in the battery, can be described by the following difference equation:

$$s(i+1) = s(i) + q_c(i)\gamma_e - \frac{q_d(i)}{\gamma_e} \tag{1}$$

where i is the time window index, $s(i)$ denotes the energy stored in the battery at the beginning of the ith time window, $q_c(i)$ and $q_d(i)$ are the energy charged to and discharged from the battery at time window i, respectively, and γ_e denotes the energy efficiency, which represents the energy loss in the battery. We have $\gamma_e = \gamma_{\text{inv}}\sqrt{\gamma_{\text{batt}}}$, where γ_{inv} is the inverter efficiency and γ_{batt} is the battery round-trip efficiency [20].

Due to the physical limits of the battery, the average charging and discharging rates at any time window are limited by the number of batteries and the physical limit of each battery as

$$0 \le q_c(i) \le n_b Q_c \tau \quad \forall i \in \mathcal{H} \tag{2}$$

$$0 \le q_d(i) \le n_b Q_d \tau \quad \forall i \in \mathcal{H} \tag{3}$$

where n_b is the number of batteries, Q_c and Q_d are the maximum charging and discharging power of a single battery, respectively, and $\mathcal{H} = \{1, 2, \ldots, H\}$ is the time horizon under consideration, with H being the total number of time windows.

In addition to the charging and discharging limits, the SOC at any time is limited by the total capacities of the battery as

$$0 \le s(i) \le n_b S[1 - \alpha \cdot (m-1)^{0.75} - \beta\sqrt{m-1}] \tag{4}$$

where S is the initial battery capacity, or the maximum energy, of a single battery, α and β are the calendar aging and cycling aging coefficients of the battery described in months, respectively, and m is the age of the battery in months [21]. The aging coefficient models the phenomenon that the battery capacity becomes smaller over a long period of time.

B. Power From the Grid

Denote $q^{\text{net}}(i)$ as the energy bought from the utility at time window i. Then, we have

$$q^{\text{net}}(i) = q^{\text{ld}}(i) - q^{\text{sol}}(i) + q_c(i) - q_d(i) \tag{5}$$

where $q^{\text{ld}}(i)$ denotes the actual load at time window i, and $q^{\text{sol}}(i)$ denotes the PV energy collected from the solar panels at time window i. The PV energy can be modeled as

$$q^{\text{sol}}(i) = n_s q_0(i) \gamma_s^{m-1} \tag{6}$$

where n_s is the number of solar panels, $q_0(i)$ is the PV energy collected by a single panel at time window i, γ_s is the efficiency of the solar panel described in months, m is the age of the solar panel in months. The solar panel efficiency describes the aging effect of the solar panel over time.

C. Objective Function

The total cost of the system consists three parts—energy charge, power or demand charge, and system cost.

1) Energy Charge: Time of use (TOU) is a rate plan that is determined by both the amount of energy bought from the utility and the time when the energy is consumed. Despite slight differences in the rate between utilities, most TOU plans divide days into peak hours, part-peak hours, and off-peak hours. Similarly, weeks are divided into weekdays and weekends; years are divided into summer months and winter months.

Define the set of peak hours, part-peak hours, and off-peak hours as $\mathcal{H}_{\text{pk}}$, $\mathcal{H}_{\text{pp}}$, and $\mathcal{H}_{\text{op}}$, respectively. Denote the electricity cost during these three sets of hours as P_{pk}, P_{pp}, and P_{op}, respectively. Considering the effects of inflation, the unit price (\$/kWh) at time window i is given by

$$P(i) = \begin{cases} P_{\text{pk}}\left(1 + r_{\text{infl}}^{\lfloor \frac{i-1}{W} \rfloor}\right), & i \in \mathcal{H}_{\text{pk}} \\ P_{\text{pp}}\left(1 + r_{\text{infl}}^{\lfloor \frac{i-1}{W} \rfloor}\right), & i \in \mathcal{H}_{\text{pp}} \\ P_{\text{op}}\left(1 + r_{\text{infl}}^{\lfloor \frac{i-1}{W} \rfloor}\right), & i \in \mathcal{H}_{\text{op}} \end{cases} \tag{7}$$

where r_{infl} is the annual inflation rate of electricity cost, W is the total number of windows in one year, and the floor operator $\lfloor a \rfloor$ returns the largest integer that is less than or equal to a.

Define $\mathcal{H}_m$ as the set of time window indices that belong to the mth month, and assume there are M months in the time horizon $\mathcal{H}$, that is, $\mathcal{H} = \bigcup_{m=1}^{M} \mathcal{H}_m$. The energy charge with the given TOU is

$$C_{\text{E}} = \sum_{m=1}^{M} \sum_{i \in \mathcal{H}_m} P(i) \max\left(q^{\text{net}}(i), 0\right). \tag{8}$$

2) Demand Charge: The demand charge is proportional to the highest average power in each month. Considering the effects of inflation, denote the demand charge at the mth month

$$D_{\max}(m) = D_0 \cdot \left(1 + r_{\text{infl}}^{\lfloor \frac{m-1}{12} \rfloor}\right) \tag{9}$$

where D_0 is the initial demand charge in the unit of \$/kW.

The total demand charge can be calculated as

$$C_{\text{D}} = \sum_{m=1}^{M} D_{\max}(m) \max_{i \in \mathcal{H}_m} \frac{q^{\text{net}}(i)}{\tau}. \tag{10}$$

3) System Cost: The costs of solar panels and batteries include the costs for product procurement, installation, and maintenance. It is assumed that the total cost is proportional to the number of solar panels and batteries as

$$C_{\text{S}} = P_s n_s + P_b n_b \tag{11}$$

where P_s and P_b are the unit costs (including procurement and installation) of solar panels and batteries, respectively, and n_s and n_b are the number of solar panels and batteries, respectively.

D. Problem Formulation

The objective of the problem is to minimize the long-term total cost of the system by identifying the optimum number of solar panels and batteries required for the system. The optimum identification of the solar panels and batteries depends on the charging and discharging schedule; thus, the charging and discharging rates $q_c(i)$ and $q_d(i)$, for all $i \in \mathcal{H}$, will also be considered as optimization variables.

Since the optimum design is performed off-line before system installation, the load information $q^{\text{ld}}(i)$ and the solar energy $q^{\text{sol}}(i)$ are unknown during the design phase. However, the optimum design can be performed by using known historical data given that the load and weather for a given location do not change dramatically from year to year [5]. Thus, the known historical data of $q^{\text{ld}}(i)$ and $q^{\text{sol}}(i)$ are used in the optimum design as in [5].

Based on the abovementioned models and analysis, the optimization problem can be formulated as

$$\begin{aligned} \text{(P1)} \quad \min. \quad & C_{\text{E}} + C_{\text{D}} + C_{\text{S}} && (12) \\ \text{s.t.} \quad & (1)-(6) && (13) \\ & n_s, n_b \in \mathbb{Z}_+ && (14) \\ & n_s \le N_s && (15) \\ & n_b \le N_b && (16) \end{aligned}$$

where $\mathbb{Z}_+$ is the set of nonnegative integers, N_s and N_b are the maximum number of solar panels and batteries allowed in the system, respectively, and the optimization is performed with respect to the following variables: $\{q_c(i), q_d(i)\}_{i \in \mathcal{H}}$, n_s, and n_b. The values of N_s and N_b are usually determined by the area of installation.

The abovementioned problem is an MINLP problem. The nonlinearity comes from the maximum term in both the energy charge C_{E} in (8) and the demand charge C_{D} in (10). The problem is in general NP-hard.

III. Mixed Integer Linear Programming

In this section, we transform (P1) into an equivalent MILP problem [13], which can be optimally solved by using the B&B algorithm [22].

Since the nonlinearity in (P1) comes from the maximum term in the objective function, we can equivalently convert it to a linear objective function by introducing new variables [23]. Define two new variables $q_+^{\text{net}}(i)$ and $q_{\max}^{\text{net}}(m)$ with the following new constraints:

$$q^{\text{net}}(i) \le q_+^{\text{net}}(i) \quad \forall i \in \mathcal{H} \tag{17}$$

$$q^{\text{net}}(i) \le q_{\max}^{\text{net}}(m) \quad \forall i \in \mathcal{H}_m \tag{18}$$

$$q_+^{\text{net}}(i) \ge 0 \quad \forall i \in \mathcal{H} \tag{19}$$

$$q_{\max}^{\text{net}}(m) \ge 0 \quad \forall m \in \mathcal{M} \tag{20}$$

where $\mathcal{M} = \{m | \mathcal{H}_m \subseteq \mathcal{H}\}$ is the set of indices of months in the optimization time horizon.

Based on the abovementioned definition and constraints, the energy charge and demand charge can be upper bounded, respectively, by

$$\bar{C}_{\text{E}} = \sum_{m=1}^{M} \sum_{i \in \mathcal{H}_m} P(i) q_+^{\text{net}}(i) \tag{21}$$

$$\bar{C}_{\text{D}} = \frac{1}{\tau} \sum_{m=1}^{M} D_{\max}(m) q_{\max}^{\text{net}}(m). \tag{22}$$

The MINLP problem (P1) can now be equivalently converted to a new problem as

$$\text{(P2)} \quad \min \quad \bar{C}_{\text{E}} + \bar{C}_{\text{D}} + C_{\text{S}} \tag{23}$$

$$\text{s.t.} \quad (1)-(6), (14)-(20) \tag{24}$$

where the optimization variables are: $\{q_c(i), q_d(i), q_+^{\text{net}}(i)\}_{i \in \mathcal{H}}$, $\{q_{\max}^{\text{net}}(m)\}_{m \in \mathcal{M}}, n_s$, and n_b. Compared to (P1), (P2) has two new groups of optimization variables, $\{q_+^{\text{net}}(i)\}_{i \in \mathcal{H}}$ and $\{q_{\max}^{\text{net}}(m)\}_{m \in \mathcal{M}}$. The energy and demand charges in (P1) are replaced in (P2) with their respective upper bounds, which are linear functions of the optimization variables. As a result, the nonlinearity in (P1) is removed and (P2) is an MILP.

The equivalence between (P1) and (P2) is established in the following lemma.

Lemma 1: The optimum solution to (P2) is also the optimum solution to (P1).

Proof: Denote the optimum cost functions from (P1) and (P2) as $C_{\text{E}}^* + C_{\text{D}}^* + C_{\text{S}}^*$ and $\bar{C}_{\text{E}}^\dagger + \bar{C}_{\text{D}}^\dagger + C_{\text{S}}^\dagger$, respectively. Since $C_{\text{E}} \le \bar{C}_{\text{E}}$ and $C_{\text{D}} \le \bar{C}_{\text{D}}$ by definition, we have $C_{\text{E}}^* \le \bar{C}_{\text{E}}^\dagger$ and $C_{\text{D}}^* \le \bar{C}_{\text{D}}^\dagger$.

Next, we will show that $C_{\text{E}}^* = \bar{C}_{\text{E}}^\dagger$ and $C_{\text{D}}^* = \bar{C}_{\text{D}}^\dagger$ by using contradiction. Assume $C_{\text{E}}^* < \bar{C}_{\text{E}}^\dagger$ and $C_{\text{D}}^* < \bar{C}_{\text{D}}^\dagger$, then we can always make $\bar{C}_{\text{E}}^\dagger$ and $\bar{C}_{\text{D}}^\dagger$ smaller by letting

$$q_+^{\text{net}}(i) = \max(0, q^{\text{net}}(i)) \tag{25}$$

$$q_{\max}^{\text{net}}(m) = \max_{i \in \mathcal{H}_m} q^{\text{net}}(i) \tag{26}$$

while keeping all other variables unchanged to satisfy all constraints. Thus, we must have $C_{\text{E}}^* = \bar{C}_{\text{E}}^\dagger$ and $C_{\text{D}}^* = \bar{C}_{\text{D}}^\dagger$, and the equality is achieved when (25) and (26) are satisfied. That is, (25) and (26) give the optimum values of $q_+^{\text{net}}(i)$ and $q_{\max}^{\text{net}}(m)$ in (P2).

Substituting the optimum values of $q_+^{\text{net}}(i)$ and $q_{\max}^{\text{net}}(m)$ given in (25) and (26) into (P2), we can see that (P2) is exactly the same as (P1). Thus, the optimum solutions to the two problems are equivalent. This completes the proof. ■

The MILP problem in (P2) is still nonconvex due to the integer constraints. The MILP can be optimally solved by using the B&B algorithm [22], which performs systematic enumeration of subsets (branches) of the feasible region by iteratively dividing the current branch into two branches based on solutions of relaxed integer linear program in the current branch. The solutions in each branch are compared to the estimated upper and lower bounds of the optimal value, and a branch is discarded if it cannot outperform the best result found so far by the algorithm.

The B&B algorithm can obtain the globally optimum solution to (P2) with a complexity that is much lower than exhaustive search. The calculation in each branch requires solving an LP problem.

To accurately account for the aging effects of the battery and solar panel, the optimization needs to be performed over the entire life cycle of the battery and/or solar panels. As a result, the optimization time horizon is in the order of years or longer. For example, if the expected life cycle of a battery is ten years and we use 1-h windows, then there are a total of $H = 87\,648$ hours and $M = 120$ months if we include two leap years. As a result, the total number of optimization variables are $3H + M + 2 = 263\,066$. Even though LP can be solved in polynomial time, the large number of optimization variables makes the complexity extremely high and requires very long optimization time. In the B&B algorithm, relaxed LP needs to be performed in each branch, and this further improves the computation complexity.

IV. Low-Complexity Solution With DP

In this section, we propose to solve (P1) by developing a low-complexity algorithm with the help of DP.

The optimization variables in (P1) include the charging/discharging schedule $\{q_c(i), q_d(i)\}_{i \in \mathcal{H}}$ and the number of batteries and solar panels n_s and n_b. In order to implement DP, (P1) is decomposed into two subproblems by separating the dynamic variables $\{q_c(i), q_d(i)\}_{i \in \mathcal{H}}$ and static variables $\{n_s, n_b\}$ as

$$\text{(P1a)} \quad \min_{\{q_c(i), q_d(i)\}_{i \in \mathcal{H}}} \quad C_{\text{ED}} \triangleq C_{\text{E}}(n_s, n_b) + C_{\text{D}}(n_s, n_b)$$

$$\text{s.t.} \quad (1)-(6)$$

$$\text{(P1b)} \quad \min_{\{n_s, n_b\}} \quad C_{\text{ED}}^*(n_s, n_b) + C_{\text{S}}(n_s, n_b)$$

$$\text{s.t.} \quad n_s, n_b \in \mathbb{Z}_+$$

$$n_s \le N_s$$

$$n_b \le N_b$$

where $C_{\text{ED}}^*(n_s, n_b)$ is the optimum solution to (P1a), given n_s and n_b.

In (P1a), we first fix the static variables n_s and n_b, and minimize the energy and demand charges by identifying the optimum dynamic variables $\{q_c(i), q_d(i)\}_{i\in\mathcal{H}}$. Under a fixed n_s and n_b, the cost of battery and solar panels are fixed, so $C_{\rm S}$ is excluded from the objective function in (P1a). In the objective function, the energy and demand charges are expressed as explicit functions of n_s and n_b. With the optimum scheduling obtained from (P1a), we can then identify the optimum values of n_s and n_b in (P1b). (P1a) can be solved by using DP, and (P1b) can be solved through coordinate descent with binary search.

A. Solving (P1a) With DP

DP is based on Bellman's principle of optimality, which states that the state and decision at the current moment fully determine the optimum policy in the future. However, Bellman's principle of optimality cannot be readily applied to (P1a), mainly due to the form of the demand charge $C_{\rm D}$ in its objective function.

In the calculation of the objective function, the summation in $C_{\rm E}$ is performed in the time scale of small time windows (e.g., hours), yet the summation in $C_{\rm D}$ is performed in the time scale of months, and the maximum operator in $C_{\rm D}$ is performed over all the time windows within a month. Such maximum operations cannot be readily described by the Bellman equation. Thus, we need to transform the calculation of $C_{\rm D}$ such that it has the same time scale as the calculation of $C_{\rm E}$, and then, transform (P1a) into an equivalent problem that satisfies Bellman's principle of optimality.

Denote the indices of the first and last time windows in $\mathcal{H}_m$ as i_{m1} and i_{m2}, respectively. Then, we define a new state variable $\phi_i^{(m)}$ as

$$\phi_i^{(m)} = \begin{cases} 0, & i < i_{m1} \\ \max(\phi_{i-1}^{(m)}, q^{\rm net}(i)), & i \in \mathcal{H}_m \\ \max_{i\in\mathcal{H}_m} q^{\rm net}(i), & i > i_{m2} \end{cases}. \tag{27}$$

Based on the abovementioned definition, the demand charge in the mth month can be calculated as

$$C_{\rm D}^{(m)} = \frac{D_{\max}(m)}{\tau} \sum_{i\in\mathcal{H}_m} \left(\phi_i^{(m)} - \phi_{i-1}^{(m)}\right). \tag{28}$$

The total demand charge can then be calculated as

$$C_{\rm D} = \sum_{m=1}^{M} C_{\rm D}^{(m)} = \frac{1}{\tau}\sum_{m=1}^{M} D_{\max}(m) \sum_{i\in\mathcal{H}_m} \left(\phi_i^{(m)} - \phi_{i-1}^{(m)}\right). \tag{29}$$

From (27), we have

$$C_{\rm D} = \frac{1}{\tau}\sum_{m=1}^{M} D_{\max}(m) \sum_{i\in\mathcal{H}_m} \max(0, q^{\rm net}(i) - \phi_{i-1}^{(m)}). \tag{30}$$

The cost function in (P1a) can then be rewritten as

$$C_{\rm E} + C_{\rm D} = \sum_{m=1}^{M}\sum_{i\in\mathcal{H}_m} \Bigg[P(i)\max(0, q^{\rm net}(i)) + \frac{D_{\max}(m)}{\tau}\max(0, q^{\rm net}(i) - \phi_{i-1}^{(m)})\Bigg]. \tag{31}$$

The cost function in (31) can help us convert (P1a) into an equivalent problem that satisfies Bellman's principal of optimality. For the optimization problem, the action variable at $i \in \mathcal{H}_m$ is $a(i) = \{q_c(i), q_d(i)\}$, and the state variables are $\beta(i) = \{S(i), \phi_{i-1}^{(m)}\}$. To facilitate analysis, for $i \in \mathcal{H}_m$, define

$$r(\beta(i), a(i)) = P(i)\max(0, q^{\rm net}(i)) + \frac{D_{\max}(m)}{\tau}\max(0, q^{\rm net}(i) - \phi_{i-1}^{(m)}) \tag{32}$$

With the abovementioned definition, (P1a) can be equivalently converted to

$$\text{(P3)} \quad \min_{\{q_c(i), q_d(i)\}_{i\in\mathcal{H}}} \sum_{m=1}^{M}\sum_{i\in\mathcal{H}_m} r(\beta(i), a(i)) \quad \text{s.t.} \quad (1)-(6), (27).$$

In (P3), the cost function is decomposed as the summation of $r(\beta(i), a(i))$, which depends solely on the current state variable $\beta(i)$ and action variable $a(i)$. Constraints (1) and (27) describe the evolution of the state variables; constraints (2)–(6) specify the boundaries of the state and action variables. Thus, (P3) satisfies Bellman's principal of optimality. The Bellman equation of (P3) can be written as

$$\begin{aligned} V_0(\beta(0)) &= \min_{\{q_c(0), q_d(0)\}} r(\beta(0), a(0)) = 0 \\ V_i(\beta(i)) &= \min_{\{q_c(i), q_d(i)\}} \left[r(\beta(i), a(i)) + V_{i-1}(\beta(i-1))\right], \quad 1 \le i \le H. \end{aligned} \tag{33}$$

Specifically, the objective is to find at each time window i, the optimum value function $V_i(\beta(i))$ that corresponds to the optimum cost in the time horizon between $[1, i]$. In the abovementioned notation, $\beta(0)$ denotes the initial state at $t = 0$ and $J = V_H(\beta(H))$ is the optimal cost from the initial state to the finial state.

The optimum schedule $q_c(i)$ and $q_d(i)$ can be obtained by solving the Bellman equation in (33) through forward recursion based on the following equations:

$$(s_{\beta(i)}, a_{\beta(i)}) = \arg\min_{(s,a)\in\Omega_{\beta(i)}} \left[r(\beta(i), a) + V_{i-1}(s)\right] \tag{34}$$

where $\Omega_{\beta(i)}$ is the space that contains all state and action pairs (s, a) such that we can reach state $\beta(i)$ from $\beta(i-1) = s$ by taking action a. At time i, $a_{\beta(i)}$ gives the optimum action to reach state $\beta(i)$ by minimizing the accumulated cost from the initial state to the current state $\beta(i)$; correspondingly, $s_{\beta(i)}$ is the state preceding $\beta(i)$ with the action $a_{\beta(i)}$. Then, the value function $V_i(\beta(i))$ can be updated by

$$V_i(\beta(i)) = r(\beta(i), a_{\beta(i)}) + V_{i-1}(s_{\beta(i)}). \tag{35}$$

However, there is, in general, no closed-form solution to the Bellman equation for arbitrary state $\beta(i)$. We can numerically solve the Bellman equation by using algorithms such as relative value iteration algorithm (RVIA) [24], the Viterbi algorithm [25], or the Bellman–Ford algorithm [26]. The implementation of these algorithms requires the discretization of

the continuous state variables and action variables. A larger discretization step size can reduce the complexity at the cost of lower precision, and vice versa. The tradeoffs between complexity and accuracy have been studied in [27]–[30]. The impacts of the discretization step are studied with numerical examples in the next section, and it will be shown that an appropriate discretization step can be chosen to achieve negligible approximation errors while maintaining the low complexity of the algorithm.

The action space contains two variables $q_c(i)$ and $q_d(i)$. Thus, the size of the action space grows quadratically with the number of discretization levels of the charging/discharging action. Since the complexity of the DP algorithm is directly proportional to the size of the action and state spaces, we propose to reduce the dimension of the action space by replacing the two action variables $q_c(i)$ and $q_d(i)$ in (P3) with a single variable $q^{\text{net}}(i)$ as

$$\text{(P4)} \quad \min_{\{q^{\text{net}}(i)\}_{i\in\mathcal{H}}} \quad \sum_{m=1}^{M}\sum_{i\in\mathcal{H}_m} r(\beta(i), q^{\text{net}}(i))$$
$$\text{s.t.} \quad (1)-(6), (27).$$

The equivalence between (P3) and (P4) is established in the following lemma.

Lemma 2: The optimum solution to (P4) is also the optimum solution to (P3).

Proof: For a given pair $\{q_c(i), q_d(i)\}$, $q^{\text{net}}(i)$ is uniquely determined according to (5). On the other hand, for a given $q^{\text{net}}(i)$, we may have multiple $\{q_c(i), q_d(i)\}$. To prove the equivalence between (P3) and (P4), it is sufficient to show that the optimum $\{q_c(i), q_d(i)\}$ for (P3) can be uniquely determined by the optimum $\{q^{\text{net}}(i)\}$ for (P4), that is, there is a bijective relationship between the optimum solutions between (P3) and (P4).

Assume that there are two different pairs of action variables, $a_1(i) = (q_{c1}(i), q_{d1}(i))$ and $a_2(i) = (q_{c2}(i), q_{d2}(i))$, which provide the same transition from $\beta(i-1)$ to $\beta(i)$ in the discretized state space. By definition

$$q_{c1}(i)\gamma_e - \frac{q_{d1}(i)}{\gamma_e} = q_{c2}(i)\gamma_e - \frac{q_{d2}(i)}{\gamma_e} = S(i) - S(i-1) \quad (36)$$

then, we have

$$(q_{c1}(i) - q_{c2}(i))\gamma_e = \frac{q_{d1}(i) - q_{d2}(i)}{\gamma_e}. \quad (37)$$

Without loss of generality, assume $q_{c1}(i) > q_{c2}(i)$. Given the fact that $0 < \gamma_e < 1$, we have

$$q_{c1}(i) - q_{c2}(i) > q_{d1}(i) - q_{d2}(i)$$
$$q_{c1}(i) - q_{d1}(i) > q_{c2}(i) - q_{d2}(i)$$
$$q_1^{\text{net}}(i) > q_2^{\text{net}}(i).$$

Based on (32), we have

$$r(\beta(i), a_1(i)) > r(\beta(i), a_2(i)). \quad (38)$$

Then, according to (34), $a_1(i)$ cannot be the optimum solution. Thus, an optimum $q^{\text{net}}(i)$ corresponds to one unique pair of $(q_c(i), q_d(i))$. This abovementioned analysis proves the bijective relationship between the optimum $q^{\text{net}}(i)$ and $(q_c(i), q_d(i))$. This completes the proof. ■

Algorithm 1: Modified Bellman–Ford Algorithm.

Input: Step size q, discretized state space $\mathcal{B}$, discretized action space $\mathcal{A}$, cost function $r(s,a)\ \forall s \in \mathcal{B}, a \in \mathcal{A}$.

1: **Initialization:** set the initial state $\beta(0) = 0$, the initial value function $V_0(\beta(0)) = 0$.
2: **for** $i = 1$ **to** H **do**
3: **for** $\beta(i) \in \mathcal{B}$ **do**
4: Find the optimal (previous state, action) pair that can reach $\beta(i)$

$$(s_{\beta(i)}, a_{\beta(i)}) = \underset{(s,a)\in\Omega_{\beta(i)}}{\arg\min} \ [r(\beta(i), a) + V_{i-1}(s)]$$

5: Compute the value function

$$V_i(\beta(i)) = r(\beta(i), a_{\beta(i)}) + V_{i-1}(s_{\beta(i)})$$

6: **end for**
7: **end for**
8: Identify the optimum ending state $\beta^*(H) = \arg\min_{\beta(H)\in\mathcal{B}} V_H(\beta(H))$
9: Identify the optimum actions and states at each iteration by tracing back from the the optimum ending state

$$a^*(i-1) = a_{\beta^*(i)},\ \beta^*(i-1) = s_{\beta^*(i)},\ \text{for } i = H, \ldots, 2$$

Output: Optimum policy $a^*(i)$, for $i = 1, \ldots, H-1$.

Based on the equivalence between (P3) and (P4), we can solve (P4) by using the scalar variable $q^{\text{net}}(i)$ as the action variable during the numerical solution of the Bellman equation with (34) and (35). The Bellman equation is solved with a modified Bellman–Ford algorithm, and the details are given in Algorithm 1.

B. Solving (P1b) With Coordinate Descent (CD)

The CD algorithm is used to solve the optimum values of n_b and n_s by using the results of the DP algorithm in the previous subsection. The CD algorithm is implemented by using relaxed integer programming (RIP) of (P1), where we remove the integer constraint $n_b, n_s \in \mathbb{Z}_+$. The integer-relaxed version of (P1) forms a convex problem, because it contains only linear and maximum operators of the optimization variables: n_s, n_b, and $\{q_c(i), q_d(i)\}_{i\in\mathcal{H}}$.

The CD algorithm is summarized in Algorithm 2. In the algorithm, $C^*_{\text{ED}}(n_s, n_b)$ is the optimum solution to (P1a) according to Algorithm 1.

Since the integer-relaxed version of (P1) is convex, it is convex in each individual variable. Thus, CD can be performed to identify the integer-relaxed optimum solution of n_s and n_b by successively minimizing along coordinate directions. In each iteration, we fix the value of one variable and identify the optimum value of the other. Given the fact that the objective function is convex in n_s and n_b, the optimization in each direction can be performed by using binary search. The implementation of binary

Algorithm 2: CD Algorithm to Compute n_b and n_s.

Input: Step size q.

1: **Initialization:** Iteration counter $k \leftarrow 0$, and $n_b^{(0)} \leftarrow N_b$, $n_s^{(0)} \leftarrow N_s$.

2: **repeat**

3: Identify the value of $n_s^{(k+1)}$: Using binary search to solve

$$n_s^{(k+1)} = \arg\min_{n_s} \left\{ C_{\text{ED}}^* \left(n_s, n_b^{(k)} \right) + P_s n_s + P_b n_b^{(k)} \right\}$$

4: Identify the value of $n_b^{(k+1)}$: Using binary search to solve

$$n_b^{(k+1)} = \arg\min_{n_b} \left\{ C_{\text{ED}}^* \left(n_s^{(k+1)}, n_b \right) + P_s n_s^{(k+1)} + P_b n_b \right\}$$

5: $k \leftarrow k + 1$.

6: **until** $|n_b^{(k+1)} - n_b^{(k)}| < 1$ and $|n_s^{(k+1)} - n_s^{(k)}| < 1$.

7: Rounding the solution $n_s^\dagger = n_s^{(k+1)}$ and $n_b^\dagger = n_b^{(k+1)}$ to their nearest integer values.

Output: The optimal size $n_b^\dagger$ and $n_s^\dagger$, the total cost $C_{\text{ED}}^*(n_s^\dagger, n_b^\dagger) + P_s n_s^\dagger + P_b n_b^\dagger$

search requires an upper bound on the values of n_b and n_s, and both can be upper bounded by the area of installation as in (15) and (16).

Due to the convexity of the integer-relaxed optimization problem, the CD algorithm will converge to the integer-relaxed optimum solutions upon convergence. Denote the optimum solution to the integer-relaxed optimization problem as $n_s^\dagger$ and $n_b^\dagger$. Then, the integer solution can be obtained by rounding $n_s^\dagger$ and $n_b^\dagger$ to their nearest integer values. It should be noted that the final integer solution might be suboptimum due to rounding of the solution of RIP.

V. Case Studies

Case studies are performed in this section to demonstrate the performance of the optimum designs of PV system with BESS. The designs are performed by using load data from a public database provided by the Office of Energy Efficiency and Renewable Energy (EERE) at the U.S. Department of Energy (DOE) [19]. The database provides hourly load data in one year from different types of buildings at various locations. The data from a large hotel building in San Francisco in 2004 are used in this article. The energy provided by solar panels is estimated by using the PVWatts calculator [31] from National Renewable Energy Laboratory (NREL). The utility charges are calculated by using the TOU rate $(P(i), D_0)$ of Pacific Gas and Electric Company (PG&E) in Table I, along with the time division in Table II [32]. The size of the time window is set at $\tau = 1$ h. The inflation rate of electricity cost is $r_{\text{infl}} = 2\%$.

The batteries are modeled by using Tesla Powerwall, which has a charging/discharging rate of $Q_c = Q_d = 5$ kW, and a capacity of $S = 13.5$ kWh, at a price of $P_b = \$5900$ each. Based on the datasheet [33] and calculation, the energy efficiency of the batteries is $\gamma_e = 94\%$. According to the warranty on the datasheet, the calendar aging coefficient is $\alpha = 0.0036$ and the cycling aging coefficient is $\beta = 0.0155$. The initial SOC of battery in the system is 0.

TABLE I
TOU Rate in San Francisco

Total Energy Rates ($ per kWh)	Peak	Part-Peak	Off-Peak
Summer	0.15384	0.11333	0.08651
Winter	-	0.10779	0.09317
Total Demand Rates ($ per kW)	16.08		

TABLE II
Times of the Year and Times of the Day

Service Time	Summer (5/1 to 10/31)	Winter (11/1 to 4/30)
Peak	13:00 to 19:00	-
Part-Peak	10:00 to 13:00 and 19:00 to 22:00	10:00 to 22:00
Off-Peak	22:00 to 10:00	

The price of a 10-kW solar panel is set at $P_s = \$6400$, including the price of products and installation. A maximum of $N_s = 120$ panels can be installed on the hotel rooftop limited by the area. Similarly, it is assumed that a maximum of $N_b = 100$ batteries can be installed in the system. The storage efficiency for solar panels described in a month is set at $\gamma_s = 99.96\%$ [34].

To evaluate the profitability, the savings in monthly bills are discounted with an annual interest rate (r_{intr}) of 4% to calculate the net present value (NPV) up to the Mth month

$$\text{NPV} = \sum_{m=1}^{M} C_{\text{saving}}(m) \cdot (1 + r_{\text{intr}})^{\lfloor \frac{m-1}{12} \rfloor}. \tag{39}$$

The break-even point is defined as the month up to which the NPV of savings covers the total system cost for the first time.

A. One-Year Results With MILP

We first study the optimum designs of the PV system with MILP. Due to the high complexity of MILP, the design is restricted to a time horizon of one year. Optimum designs with longer time horizons will be performed by using DP and CD later this section. Due to the short time horizon, the unit prices for solar panels and batteries are prorated to one year in the cost function. That is, based on the assumption of a ten-year life cycle of the solar panels and batteries, the unit price used in the cost function in the one-year study is obtained by dividing their actual prices by a factor of ten. The optimization is performed by solving the MILP defined in (P2). The optimization results indicate that the optimum performance can be achieved by using

TABLE III
ANNUAL UTILITY BILL UNDER DIFFERENT CONFIGURATIONS

System	Battery-assisted PV	PV-only
Utility bill ($)	361,030	446,413
Savings in bill ($)	252,561	167,178
Reduction in bill	41.2%	27.2%
Electricity bill without PV ($)	613,591	

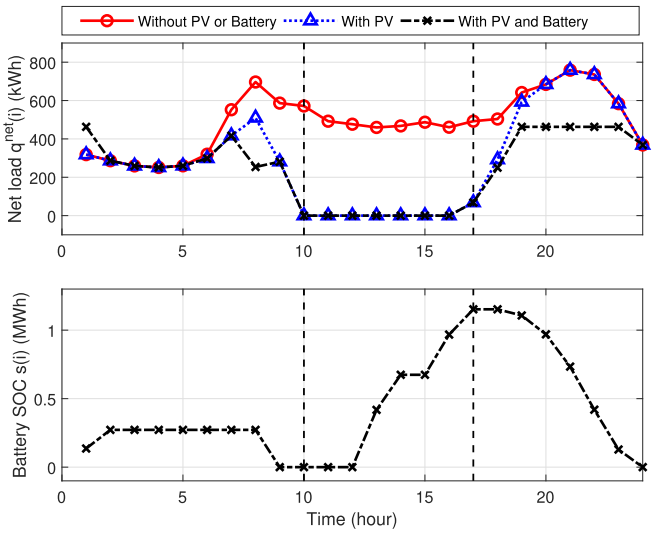

Fig. 1. Snap shot of one-day energy usage on July 1st.

$n_b^* = 90$ Tesla Powerwall batteries and $n_s^* = 120$ 10 kW solar panels in the PV system. The total saving in annual utility bills after optimization are shown in Table III. For reference, we also compare the performance of a system with solar panels but without batteries. The proposed optimum design of the battery-assisted PV system can achieve a 41.2% reduction in utility bills. For the PV-only system, the savings in utility bill drops to 27.2%.

Fig. 1 shows a snapshot of energy usage on a single day, July 1st, with or without the proposed PV system. The top figure shows the net load $q^{\text{net}}(i)$, which is the actual amount of energy bought from the utility at the ith hour; the bottom figure shows the battery SOC $s(i)$. Both are shown as functions of the hour of the day. Throughout the day, the proposed system with both PV and battery has the lowest net load, followed by the PV-only and conventional systems, respectively. The largest energy saving is achieved between 10:00 and 16:00, where the net load drops to zero because the generated solar energy exceeds the actual load. During this time period, the extra energy is charged to the battery. During the evening hours between 19:00 and 24:00, the battery is gradually discharged in the proposed system, which maintains a steady net load at 450 kWh. The battery is depleted at 24:00 because of the low energy usage after that. On the other hand, for the conventional or PV-only systems, the load is peaked at 780 kW at 21:00. Therefore, a considerable amount of energy is saved with the proposed optimum design.

Fig. 2(a) and (b) shows one-week snapshots of energy usage during the first week of June and December, respectively. Due to the relatively mild weather in San Francisco, the loads in June and December are similar. There are usually two peaks in one day—the early one is around 08:00 and the later one is around 20:00. The loads with PV in summer are much lower than that in winter especially on the early peak. The integration of solar and PV can achieve significant peak shaving. In both months, the peak of the original load is around 780 kW, and it is shaved to 480 and 510 kW in June and December, respectively. Even though employing PV without batteries can achieve similar performance as the battery-integrated PV system during day time, the omission of batteries results in the same peak as the conventional system in the evening hours, when the energy demand is the highest.

Both figures have a significant peak shaving phenomenon after using batteries. The difference between the peaks of PV-only and battery-integrated PV systems corresponds to batteries' discharging rate. In these two figures, the load difference is about 300 kW, which is smaller than the maximum discharging rate of 90 Tesla Powerwall batteries. The area between the curves of battery-integrated PV system and PV-only system is equal to the amount of energy discharged from the batteries.

B. Comparison Between Results From MILP and DP

Next, we compare the results obtained from MILP and DP in terms of both accuracy and complexity. Due to the high complexity of MILP, the comparison is performed by optimizing the system over a time horizon of one year. Since DP relies on discretization of the battery capacity and RIP is employed in CD, the results in DP are suboptimum compared to their MILP counterparts.

Fig. 3 shows monthly bills in a year with optimizations performed by using MILP and DP, respectively. In DP, the battery capacity is discretized by using a step size of $q = 10$ kWh. Both MILP and DP obtain the same optimization results for the number of Tesla Powerwall batteries $n_b^* = 90$, and the number of 10 kW solar panels $n_s^* = 120$. The scheduling results of DP and MILP are different due to the discretization approximation employed by DP. The results obtained from DP and MILP are very close to each other. It should be noted that the bills obtained by MILP in some months are higher than those from DP, but the results from MILP always yield the lowest annual bill, which is the objective function of MILP.

We can increase the precision of DP by reducing the step size q, at the cost of a higher complexity. Thus, the tradeoff between accuracy and complexity of DP can be adjusted by tuning the discretization step size q. Table IV shows the percentage error of the DP results compared to the MILP results under different step sizes q. The percentage error increases in q as expected. Using a step size of $q = 10$ kWh or less can ensure that the approximation error is below 3%. With 90 Tesla Powerwall batteries and $q = 10$ kWh, the battery capacity is discretized into $90 \times 13.5/10 = 121$ states.

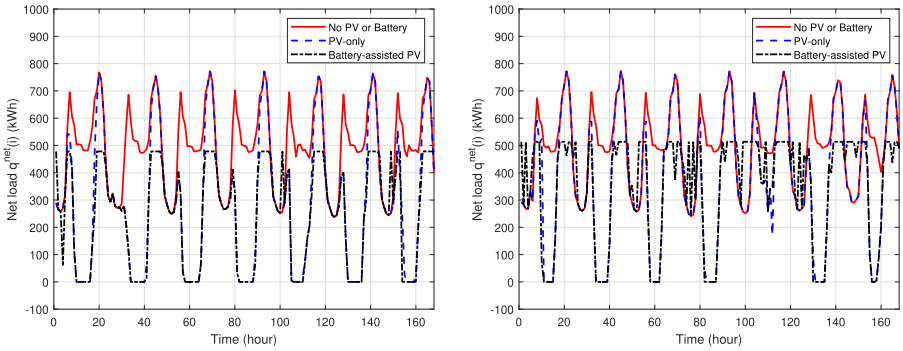

Fig. 2. Snap shots of one-week energy usage in the first weeks of June and December, respectively. (a) First week of June. (b) First week of December.

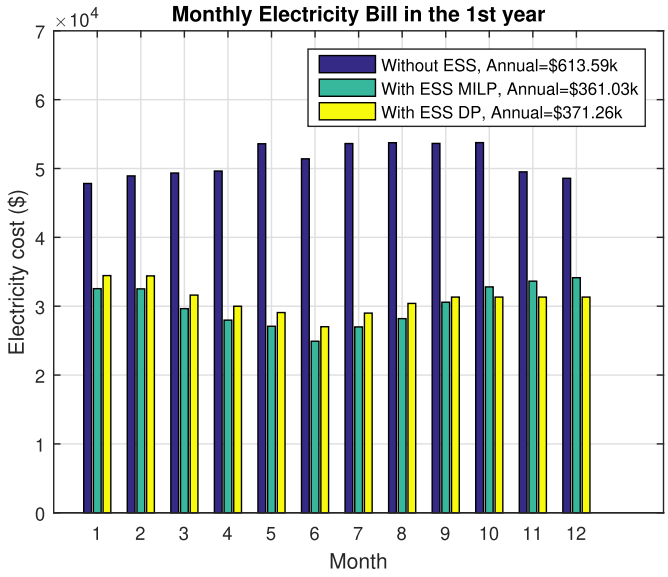

Fig. 3. Comparison of monthly electricity bill with different scheduling approaches ($q = 10$ kWh).

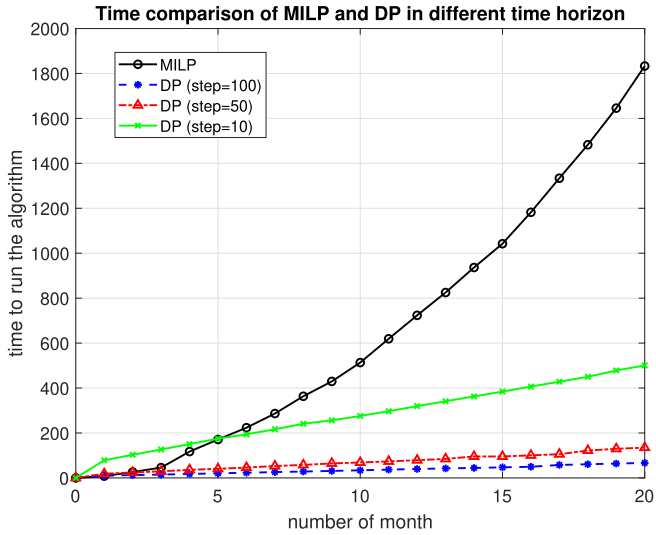

Fig. 4. Time to run the MILP and DP ($q = 10, 50,$ and 100 kWh).

TABLE IV
ERROR OF DP FOR DIFFERENT STEP SIZE

Step size q (kWh)	5	10	20	25	50	100
Annual bill (k$)	365.45	371.56	372.61	373.49	375.59	395.83
Percent error (%)	1.22	2.92	3.21	3.45	4.03	9.64

Fig. 4 compares the complexity of MILP and DP algorithm as a function of the number of months in the optimization horizon. The complexity is measured as the amount of time (in seconds) required to solve the optimization problem. All optimizations are performed on a workstation with a 6-core Intel Core i7-5820 K CPU operating at 3.3 GHz and 32 GB of random access memory (RAM). The complexity of MILP scales exponentially with m, the number of months in the time horizon. The complexity quickly becomes prohibitively high when the optimization horizon is long. On the other hand, the complexity of DP scales linearly with the number of months in the optimization horizon. The slope of the linearly scaled complexity increases as the step size q decreases. For a time horizon of 20 months, the optimization time required by MILP and DP with $q = 10$ kWh is 500.5 and 1833.0 s, respectively. The complexity difference will further increase over longer time horizons.

C. Ten-Year Results With DP

In this subsection, optimizations are performed over a time horizon of ten years with the DP algorithm, and this corresponds to $H = 87\,648$ h. A period of ten years is roughly on the same time scale as the life cycle of solar panels and batteries. Consequently, results obtained by optimizing over a ten-year time horizon can be better tuned based on the aging effects of the solar panels and batteries. However, the complexity of MILP is prohibitively high over a ten-year period, therefore, only results from DP are shown. In DP, the step size is set at $q = 10$ kWh to achieve a balanced tradeoff between complexity and accuracy. Based on the optimization results, $n_b^* = 96$ Tesla Powerwall

TABLE V
UTILITY AND SYSTEM COST UNDER TEN-YEAR HORIZON

System	Battery-assisted PV	PV-only
Utility bill ($)	3,665,409	5,075,923
Savings in bill ($)	3,402,434 (48.1%)	1,991,920 (28.2%)
System cost ($)	1,334,400	768,000
Break-even point (month)	66	51
Total cost (utitlity + system) ($)	4,999,809	5,843,923
Total saving (utitlity + system) ($)	2,068,034 (29.3%)	1,223,920 (17.3%)
Electricity bill without PV ($)	7,067,843	

batteries and $n_s^* = 120$ 10 kW solar panels are required for the PV system. Compared to the one-year optimization results, six more Tesla Powerwall batteries are required to compensate for the decrease in both efficiency and storage capacity. The number of solar panels remains unchanged at the maximum number allowed by the area of the installation site.

The total utility bills under different system configurations over the ten-year period are shown in Table V. The corresponding system costs are also shown in the table. If we do not consider the system cost, the battery-assisted PV system and PV-only system achieve a 48.1% and 28.2% reduction in the total utility bills, respectively. The savings are substantial and much greater than the cost of solar panels and/or batteries. The battery-assisted PV system and the PV-only system achieve the break-even points at the 66th and 51st month, respectively.

In addition, the battery-assisted PV system significantly outperforms the PV-only system, and the extra savings in utility bill due to the addition of batteries far exceed the cost of batteries. For example, the battery-assisted PV system costs $566 400 more than the PV-only system, yet it can achieve an additional $1 410 514 saving in the ten-year utility bill. The total costs, which include both utility bill and system cost, of the battery-assisted PV and PV-only systems are $4 999 809 and $5 843 923, respectively, which are 29.3% and 17.3% lower than the total cost of the system without PV.

The impacts of the cost of batteries and solar panels are studied in Figs. 5 and 6. Fig. 5 shows the optimum number of solar panels as a function of the PV unit price, under various values of BESS unit price. When the PV unit price is low, e.g., under $4000 per panel, then the system always selects the maximum number of solar panels allowed by the system to take advantage of low-cost solar energy. The optimum number of solar panels decreases as the PV unit price increases. Under a given PV unit price, a higher battery unit price results in more solar panels, because the system needs more solar energy to compensate for the smaller battery capacity due to higher batter cost. Similar trends are also observed for the optimum number of batteries, which decreases in battery unit price but increases in PV unit price.

Fig. 6 demonstrates the impacts of PV and battery prices on the total ten-year cost of the system. Under a given battery unit price, the total ten-year cost increases almost linearly with the

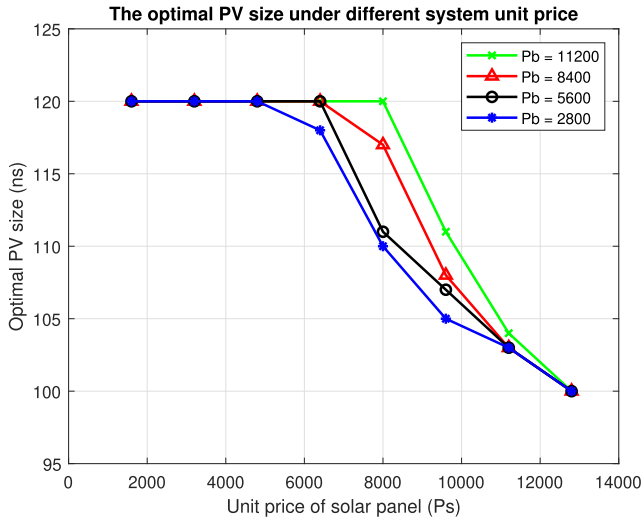

Fig. 5. Change of solar panels under different unit price.

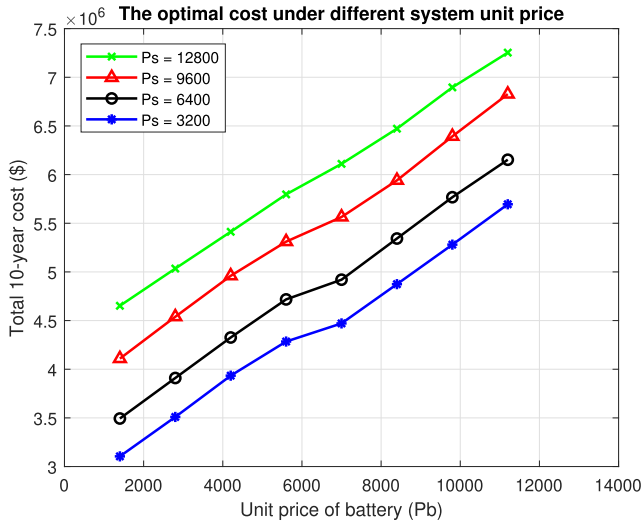

Fig. 6. Change of total cost under different unit price of the battery and solar panel.

PV unit price. The rate of increasing is not affected by the battery unit price. A similar linear relationship is also observed between the total cost and battery unit price under a fixed PV unit price.

VI. CONCLUSION

The optimum designs of PV systems with BESSs were studied in this article. In order to accurately model and quantify the impacts of aging effects of solar panels and batteries, the optimum designs were performed over a long time horizon covering the entire life cycles of the battery-assisted PV systems. MILP- and DP-based methods have been proposed to solve the optimization problem. The MILP-based solution can obtain the globally optimum solution, but with prohibitively high complexity over long optimization time horizon. The DP-based solution provided a balanced tradeoff between accuracy and complexity. Case studies with real-world data demonstrated that employing batteries in a PV system can achieve significant peak

shaving and energy saving. Over a ten-year period, the total costs of a battery-assisted PV system and PV-only system are 29.3% and 17.3% lower than a conventional system without PV.

REFERENCES

[1] J. Collins, "2020 solar power: California officially codifies mandate for homes," 2018. [Online]. Available: https://www.governing.com/topics/transportation-infrastructure/tns-cali fornia-solar-power-homes.html

[2] B. Palmintier *et al.*, "On the path to sunshot: Emerging issues and challenges in integrating solar with the distribution system," Nat. Renewable Energy Lab., Golden, CO, USA, Tech. Rep. NREL/TP-5D00-65331, 2016.

[3] A. Borghetti, C. D'Ambrosio, A. Lodi, and S. Martello, "An MILP approach for short-term hydro scheduling and unit commitment with head-dependent reservoir," *IEEE Trans. Power Syst.*, vol. 23, no. 3, pp. 1115–1124, Aug. 2008.

[4] S. Chouhan, D. Tiwari, H. Inan, S. Khushalani-Solanki, and A. Feliachi, "DER optimization to determine optimum BESS charge/discharge schedule using linear programming," in *Proc. IEEE Power Energy Soc. General Meeting*, 2016, pp. 1–5.

[5] T. A. Nguyen and R. H. Byrne, "Maximizing the cost-savings for time-of-use and net-metering customers using behind-the-meter energy storage systems," in *Proc. IEEE North Amer. Power Symp.*, 2017, pp. 1–6.

[6] K. Kwan and D. Maly, "Optimal battery energy storage system (BESS) charge scheduling with dynamic programming," *Proc. Inst. Elect. Eng., Sci., Meas. Technol.*, vol. 142, no. 6, pp. 453–458, Nov. 1995.

[7] Y. Riffonneau, S. Bacha, F. Barruel, and S. Ploix, "Optimal power flow management for grid connected PV systems with batteries," *IEEE Trans. Sustain. Energy*, vol. 2, no. 3, pp. 309–320, Jul. 2011.

[8] V. Marano, G. Rizzo, and F. A. Tiano, "Application of dynamic programming to the optimal management of a hybrid power plant with wind turbines, photovoltaic panels and compressed air energy storage," *Appl. Energy*, vol. 97, pp. 849–859, Sep. 2012.

[9] R. Kamyar and M. M. Peet, "Multi-objective dynamic programming for constrained optimization of non-separable objective functions with application in energy storage," in *Proc. 55th IEEE Conf. Decis. Control*, 2016, pp. 5348–5353.

[10] Y. Choi and H. Kim, "Optimal scheduling of energy storage system for self-sustainable base station operation considering battery wear-out cost," *Energies*, vol. 9, no. 6, Jun. 2016, Art. no. 462.

[11] M. Jones and M. M. Peet, "Solving dynamic programming with supremum terms in the objective and application to optimal battery scheduling for electricity consumers subject to demand charges," in *Proc. IEEE 56th Annu. Conf. Decis. Control*, 2017, pp. 1323–1329.

[12] H. Dagdougui, R. Minciardi, A. Ouammi, M. Robba, and R. Sacile, "A dynamic decision model for the real-time control of hybrid renewable energy production systems," *IEEE Syst. J.*, vol. 4, no. 3, pp. 323–333, Sep. 2010.

[13] Y. Li and J. Wu, "Optimum design of battery-assisted photo-voltaic energy system for a commercial application," in *Proc. IEEE Power Energy Soc. General Meeting*, 2019, pp. 1–5.

[14] A. T. Nguyen and S. Chaitusaney, "Optimum schedule and size of BESS in the low voltage network with high penetration of solar rooftops to maintain voltages within acceptable limit," in *Proc. 14th IEEE Int. Conf. Elect. Eng./Electron., Comput., Telecommun. Inf. Technol.*, 2017, pp. 194–197.

[15] S.-W. Hwangbo, B.-J. Kim, and J.-H. Kim, "Application of economic operation strategy on battery energy storage system at Jeju," in *Proc. IEEE PES Conf. Innov. Smart Grid Technol.*, 2013, pp. 1–8.

[16] R. T. de Salis, A. Clarke, Z. Wang, J. Moyne, and D. M. Tilbury, "Energy storage control for peak shaving in a single building," in *Proc. IEEE PES General Meeting Conf. Expo.*, 2014, pp. 1–5.

[17] J. von Appen and M. Braun, "Sizing and improved grid integration of residential PV systems with heat pumps and battery storage systems," *IEEE Trans. Energy Convers.*, vol. 34, no. 1, pp. 562–571, Mar. 2019.

[18] P. Harsha and M. Dahleh, "Optimal management and sizing of energy storage under dynamic pricing for the efficient integration of renewable energy," *IEEE Trans. Power Syst.*, vol. 30, no. 3, pp. 1164–1181, May 2015.

[19] "Commercial reference buildings," U.S. Department of Energy, Washington, DC, USA. [Online]. Available: https://www.energy.gov/eere/buildings/commercial-reference-buildings

[20] C. Truong, M. Naumann, R. Karl, M. Müller, A. Jossen, and H. Hesse, "Economics of residential photovoltaic battery systems in Germany: The case of Tesla's powerwall," *Batteries*, vol. 2, no. 2, May 2016, Art. no. 14.

[21] A. Berrueta, J. Pascual, I. S. Martın, P. Sanchis, and A. Ursua, "Influence of the aging model of lithium-ion batteries on the management of PV self-consumption systems," in *Proc. IEEE Int. Conf. Environ. Elect. Eng., IEEE Ind. Commercial Power Syst. Eur.*, 2018, pp. 1–5.

[22] I. Quesada and I. Grossmann, "An LP/NLP based branch and bound algorithm for convex MINLP optimization problems," *Comput. Chem. Eng.*, vol. 16, no. 10/11, pp. 937–947, Oct. 1992.

[23] R. Ahuja, "Minimax linear programming problem," *Oper. Res. Lett.*, vol. 4, no. 3, pp. 131–134, Oct. 1985.

[24] A. Gupta, R. Jain, and P. W. Glynn, "An empirical algorithm for relative value iteration for average-cost MDPs," in *Proc. 54th IEEE Conf. Decis. Control*, 2015, pp. 5079–5084.

[25] V. P. Pribylov and A. I. Plyasunov, "A convolutional code decoder design using Viterbi algorithm with register exchange history unit," in *Proc. IEEE Siberian Conf. Control Commun.*, 2005, pp. 13–18.

[26] R. Bellman, "On a routing problem," *Quart. Appl. Math.*, vol. 16, no. 1, pp. 87–90, 1958.

[27] P. K. Kitanidis and E. Foufoula-Georgiou, "Error analysis of conventional discrete and gradient dynamic programming," *Water Resour. Res.*, vol. 23, no. 5, pp. 845–858, May 1987.

[28] K. Ponnambalam and B. J. Adams, "Comment on "Error analysis of conventional discrete and gradient dynamic programming" by P. K. Kitanidis and Efi Foufoula-Georgiou," *Water Resour. Res.*, vol. 24, no. 6, pp. 888–889, Jun. 1988.

[29] J. Stachurski, "Continuous state dynamic programming via nonexpansive approximation," *Comput. Econ.*, vol. 31, no. 2, pp. 141–160, Mar. 2008.

[30] A. Heydari, "Theoretical and numerical analysis of approximate dynamic programming with approximation errors," *J. Guid., Control, Dyn.*, vol. 39, no. 2, pp. 301–311, Feb. 2016.

[31] *PVWatts Calculator*. 2018. [Online]. Available: https://pvwatts.nrel.gov/pvwatts.php

[32] "Electric schedule E-19: Medium general demand-metered TOU service," Pacific Gas Elect. Co., San Francisco, CA, USA. 2018. [Online]. Available: https://www.scribd.com/document/253380587/Pg-e-Electric-Schedule-E-19

[33] *Tesla Powerwall*. 2018. [Online]. Available: https://www.tesla.com/powerwall

[34] C. A. F. Fernandes, J. P. N. Torres, M. Morgado, and J. A. Morgado, "Aging of solar PV plants and mitigation of their consequences," in *Proc. IEEE Int. Power Electron. Motion Control Conf.*, 2016, pp. 1240–1247.